PAPER

Magnetoresistance oscillations in topological insulator Bi_2Te_3 nanoscale antidot arrays

To cite this article: Min Song *et al* 2015 *Nanotechnology* **26** 265301

IOP Publishing Nanotechnology
Nanotechnology 26 (2015) 265301 (6pp) doi:10.1088/0957-4484/26/26/265301

Magnetoresistance oscillations in topological insulator Bi_2Te_3 nanoscale antidot arrays

Min Song[1,6], Jiun-Haw Chu[2,6], Jian Zhou[3,6], Sefaattin Tongay[3], Kai Liu[3], Joonki Suh[3], Henry Chen[4], Jeong Seuk Kang[3], Xuecheng Zou[1] and Long You[1,5]

[1] School of Optical and Electronics Information, Huazhong University of Science and Technology, Wuhan, Hubei 430074, People's Republic of China
[2] Materials Sciences Division, Lawrence Berkeley National Laboratory, Berkeley, California 94720, USA
[3] Department of Material Science and Engineering, University of California, Berkeley, California 94720, USA
[4] Department of Chemistry, University of California, Berkeley, California 94720, USA
[5] Department of Electrical Engineering and Computer Science, University of California, Berkeley, California 94720, USA

E-mail: Jiun-Haw.Chu@stanford.edu and long@eecs.berkeley.edu

Received 17 March 2015, revised 30 April 2015
Accepted for publication 11 May 2015
Published 10 June 2015

Abstract

Nanoscale antidot arrays were fabricated on a single-crystal microflake of topological insulator Bi_2Te_3. The introduction of antidot arrays significantly increased the resistance of the microflake, yet the temperature dependence of the resistance remains metallic. We observed that small oscillations that are periodic in magnetic field B appeared on top of the weak anti-localization magnetoresistance. Since the electron coherence length at low temperature becomes comparable to the feature size in our device, we argued that the magnetoresistance oscillations are the manifestation of quantum interference induced by the nanostructure. Our work demonstrates that the transport of topological insulators could indeed be controlled by artificially created nanostructures, and paves the way for future technological applications of this class of materials.

Keywords: topological insulator, antidot array, magnetoresistance, coherence length, surface states, reactive ion etching

(Some figures may appear in colour only in the online journal)

1. Introduction

The topological insulator is a new state of matter that is characterized by insulating bulk and conducting surfaces. The conduction on the surface is provided by topologically protected surface states, which have a massless Dirac-like dispersion, with spin and momentum degree of freedom interlocked [1–3]. While unique properties of the surface states demonstrate the beauty of fundamental physics, they also provide the foundation for a wide spectrum of potential technology applications.

The surface states of topological insulators have been intensively studied by spectroscopic methods such as angle-resolved photoemission or scanning tunneling spectroscopy. However for transport experiments, the measurement of surface states has often been obstructed by the contribution from bulk carriers, which is due to the inevitable formation of natural defects. One strategy to enhance the surface conduction is to increase the surface-to-volume ratio through nanostructuring. For example, thin films [4] and nanoribbons [5] of topological insulators have been synthesized, and the surface state characters have been revealed through magneto-transport measurements.

[6] These authors contributed equally.

In this work, we demonstrate the fabrication of nanoscale antidot arrays on a single-crystal microflake of topological insulator Bi_2Te_3, and study how the transport properties are modified by the antidot array structures. The antidot array structure is distinct from all the previous sample structures in two ways. First, the sample geometry is multiply connected as opposed to singly connected as in previous cases. It is well known that nontrivial quantum interference effects could arise in multiply connected devices. Second, the large number of holes in antidot arrays create a large area of surfaces, which drastically enhance the surface-to-volume ratio of the material, amplifying the effect of the surface topological states.

2. Methodology

The Bi_2Te_3 crystals were grown by melting high purity powders (99.999%) of Bi and Te with a molar ratio of 2:3 at 850 °C in evacuated quartz tubes for 3 days. It was followed by cooling slowly to 550 °C for 8 days and then annealing for 5 days before rapidly cooling down to room temperature. The Bi_2Te_3 microflakes were then mechanically exfoliated on a Si substrate coated with 300 nm thick thermal SiO2 (purchased from MTI Corporation). Micro-scale electrodes were defined with photolithography using g-line photoresist (Microchem), followed by electron beam evaporation of 5 nm thick Ti and 95 nm Au. Typical contact resistance is around 0.1 Ω, well below the channel resistance, guaranteeing the accuracy of our 2-probe electrical measurements. After initial measurements, the same device was coated with around 300 nm thick ZEP520A as etching mask. Then we used electron-beam lithography to define a dense array of nanoholes (170 nm diameter with 30 nm spacing) on the ZEP520A mask. The sample was then introduced into a reactive ion etching chamber. We used 100 sccm CH4: Ar: H2 = 1:1:1 as the ambient etching gas, the etching power setting was 100 W, and the etching time was 100 s to ensure that the etching drilled holes completely through the thickness of the Bi2Te3 flake. After the patterning, the device was put into a heated PRS 3000 resist stripper to remove the ZEP520A. A schematic of the device is shown in figure 1(a). Transport measurements were carried out in a Quantum Design Physical Property Measurement System-14 T system, and the magnetic field was always applied normal to the flake surface.

3. Results and discussion

As-grown crystals are typically degenerate semiconductors, with a bulk carrier density around 5×10^{18} cm^{-3} and a bulk resistivity about 1.5 mΩ cm. The microflakes we exfoliated are typically 100 nm thick, in which the transport is still dominated by the bulk carriers. Figure 1(d) shows the temperature dependence of the resistance (red) for a microflake before writing the antidot arrays. The 100 nm thick square flake has a resistance around 150 Ω at room temperature.

After writing the antidot arrays, the resistance of the device increases by more than two orders of magnitude, reaching a value around 60 kΩ, as shown in figure 1(e). Since the cross-sectional area for the current path is significantly reduced after etching, it is expected that the resistance should increase due to the reduction of geometric factor. However, assuming the antidot diameter 170 nm and lattice constant of the array 200 nm, one can estimate the factor of increase G by performing the calculation:

$$G = \frac{a-d}{a} + \frac{d}{a}\int_0^{d/2} \frac{a}{\left(a - \sqrt{d^2 - 4x^2}\right)} \mathrm{d}x$$

Where a is the unit cell constant and d is the diameter, and the obtained G is about 3.5. Therefore, the 400-fold increase of resistance can only be explained by the simultaneous increase in bulk resistivity, which has gone up to 100 mΩ cm after writing the antidots.

One possible cause for such a large increase of bulk resistivity is the enhancement of surface scattering, as expected from the introduction of large and intensive antidot arrays. Another possibility is that the high-energy ions used in the ion etching process could damage the bulk of nanoflake or thin films, and hence suppress the bulk conduction. (The kinetic energy of these plasma ions is round 200 eV) [6]. On the other hand, the width of the wall separating the two adjacent antidote holes is only 30 nm, which is comparable to the depletion length of Bi_2Te_3 near the surfaces. Therefore the band bending effect could also reduce the carrier density in these regions, which effectively increase the bulk resistivity.

Figure 1(e) shows the resistance of the antidot array device as a function of temperature. Surprisingly, the temperature dependence shows an overall metallic behavior, with only a small upturn below $T = 20$ K. Since the sheet 2D resistance of the device is only half of a quantum resistance (e^2/h), one would expect the conduction is strongly localized, showing an insulating behavior. Even if we treat the device conduction as a three-dimensional transport, it has also been shown that in the $Bi_xSb_{1-x}Pb_{3-x}Se_x$ alloy the bulk channel turns into an Anderson insulating state for bulk resistivity above 30 mΩ cm [7]. The fact that we are still seeing a metallic temperature dependence might suggest that surface conduction plays a significant role, which is robust against localization. This could be a consequence of the large surface-to-volume ratio resulting from the writing of the antidot arrays.

Figure 2(a) shows magnetoresistance (*MR*) of our antidot array as a function of magnetic field from 2 to 20 K. The *MR* is positive with a cusp-like shape. Such behavior is indicative of a weak anti-localization effect. The weak anti-localization could arise from scattering off impurities with a high atomic number, or the strong spin–orbit coupling of the conducting quasi-particles [8]. For the topological insulator surface state, since the spin and momentum quantum numbers are interlocked due to the protected topological ground state, it is expected that the *MR* shows a perfect two-dimensional weak anti-localization effect, which has a ln(B) field dependence in the strong field limit [9].

However, the *MR* of the antidot arrays does not follows a ln(B) field dependence. Instead, the MR appears to have a

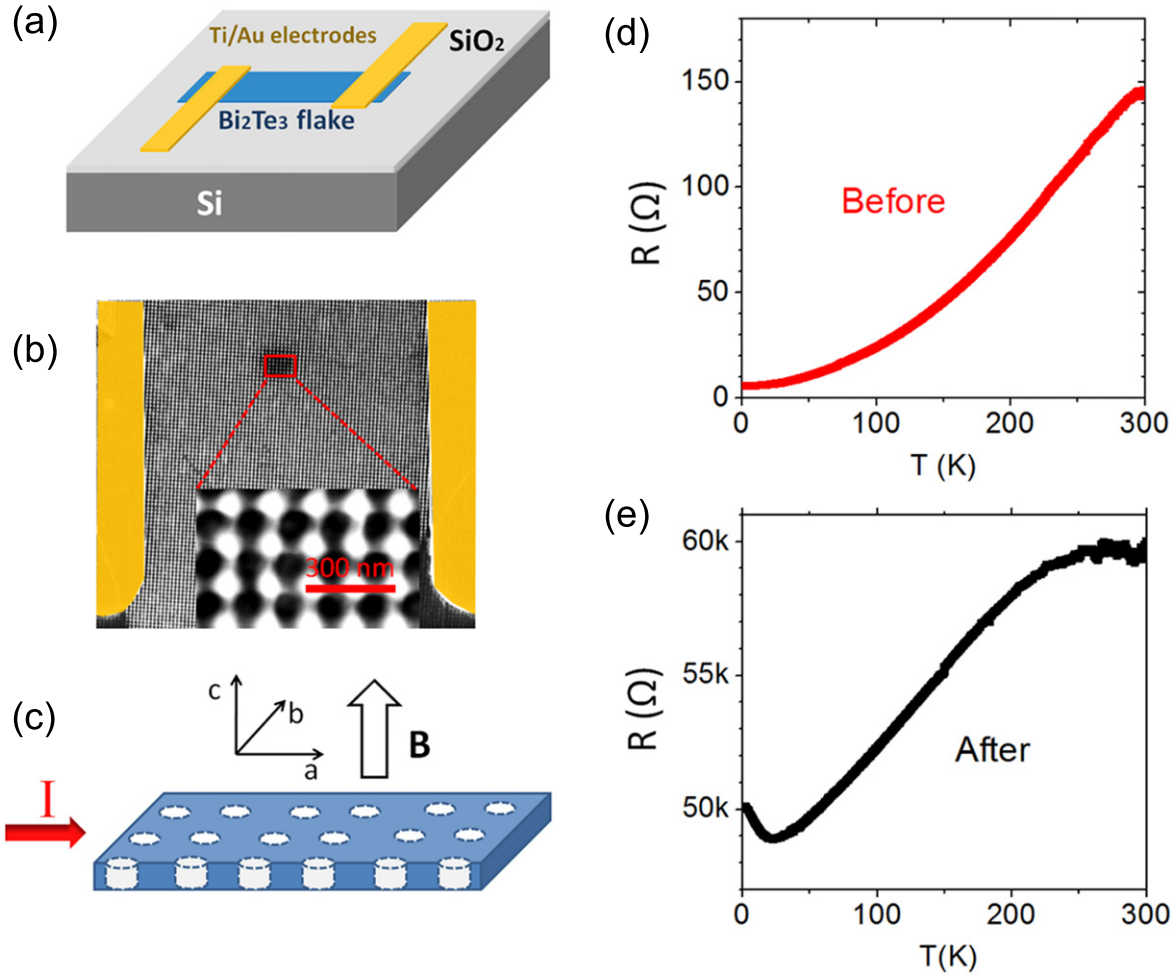

Figure 1. Device schematics and temperature-dependent transport before and after writing the antidot array. (a) Schematic of the device. The sample consists of a $6\times6\,\mu m^2$ exfoliated Bi_2Te_3 flake (100 nm thick) and two-terminal metal contacts. (b) Scanning electron microscope image of the antidot array. The array is a square lattice of holes with a 200 nm lattice constant and about 170 nm hole diameter. (c) Schematic of the structure of the antidot array. During the measurement, the magnetic field is applied along the *c*-axis of the crystal. (d) Temperature dependence of the zero-field resistance of the device before and (e) after writing the antidot array. We note the resistance of the device increases 400 fold after writing the antidot array, yet still shows metallic behavior. The small up-turn at low temperature is likely to be a result of the disorder-enhanced electron–electron interaction effect, which is commonly observed in a highly disordered system.

functional form of square root of B, as shown in figure 2(b); $B^{1/2}$ *MR* is in fact the signature of three-dimensional weak anti-localization effect instead of two-dimensional. The three-dimensional weak anti-localization can be described by the following formula [10]:

$$\frac{R(B)-R(0)}{R(B)}=\frac{\rho_0 e^2}{2\pi^2\hbar}\sqrt{\frac{eB}{\hbar}}f_3\left(\frac{4el_\varphi^2B}{\hbar}\right) \quad (1)$$

where ρ_0 is the zero filed resistivity; $\hbar$ is the Plank's constant; l_ϕ is the phase coherent length, which is the distance travelled by an electron before it loses its phase coherence; and

$$f_3(1/x)=2\left(\sqrt{2+x}-\sqrt{x}\right)-\left[\sqrt{0.5+x}+\sqrt{1.5+x}+\sqrt[2/3]{2.03+x}\right]/48$$

We fit our data by this equation, and the fitting is plotted as the thin solid curves in figure 2(a). The extracted phase coherence length as a function of temperature is shown in figure 2(c). We note that the phase coherence length of electrons exceeds 100 nm below 15 K, which is comparable to the characteristic length scale of our antidot array structure.

As we discussed above, the transport of the antidot arrays is likely dominated by the surfaces. Intuitively, one would expect a two-dimensional weak anti-localization effect to be found in the *MR*, which is inconsistent with our measurements. An explanation for this contradiction might be drawn from a recent theoretical calculation, which proposed that quantum percolation could occur in a topological insulator antidot array if the antidots are dense enough [11]. In this case, the surface states on the inner walls of the antidots could hybridize with each other and restore the bulk-like conduction; thus, the sample transport appears to be three-dimensional. We note that in this theoretical study only two-dimensional topological insulators have been considered; therefore, a generalization to three dimensions is highly desirable.

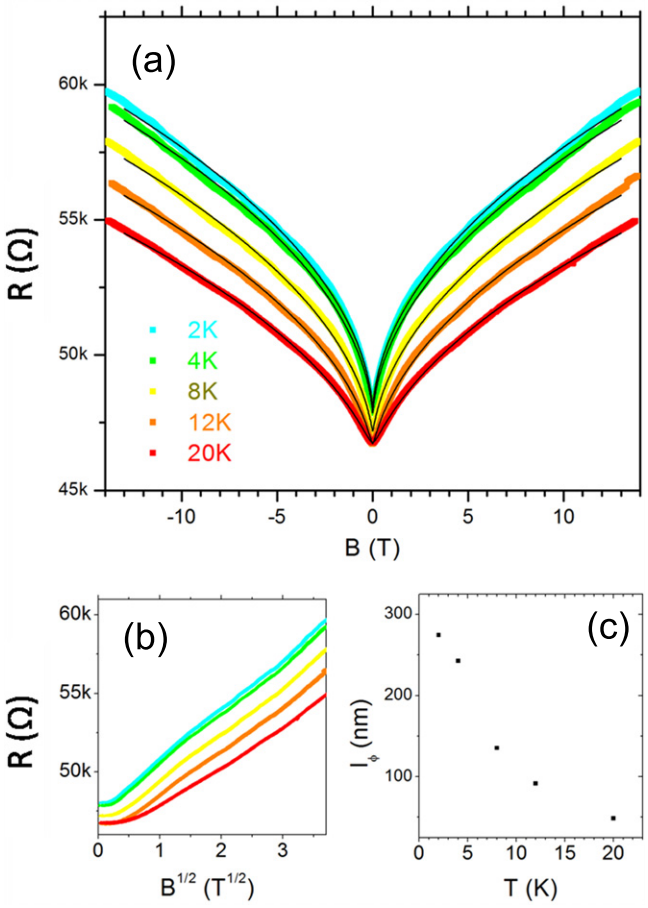

Figure 2. Magnetoresistance of the Bi_2Te_3 antidot arrays. (a) Magnetoresistance of the Bi_2Te_3 antidot arrays measured at $T = 2$ to 20 K. Thin solid curves shows the fit based on the three-dimensional weak antiloclaization theory as described in the main text. (b) Same data as (a) plotted against $B^{1/2}$. It clearly shows the magnetoresistance here scales linearly with $B^{1/2}$. (c) Coherence length l_ϕ as a function of temperature obtained from the weak antilocalization fitting.

The introduction of antidot arrays does not simply changed the resistance of the sample, it also completely modified the magneto-transport properties of Bi_2Te_3. After subtracting the smooth polynomial background[7], we extract the oscillatory parts of MR for the sample before and after writing the antidot array, and plot them in figure 3. The microflake before writing the antidot array (as shown in figure 3(a)) shows typical Shubnikov–de Haas (SdH) type oscillations, i.e. the oscillation amplitude increases at higher magnetic field (B), and the oscillation is periodic in B^{-1}, indicating typical orbit quantization in momentum space observed in the bulk and surface carriers of Bi_2Te_3 [12]. In sharp contrast, after introducing the antidot arrays, the *MR* oscillations show different behavior, as shown in figure 3(b). We find that its oscillatory *MR* consists of two features: a fast oscillating signal superimposed on a slowly varying background. Interestingly, the fast oscillating signal shows a periodic behavior in B instead of B^{-1}, with a periodicity $\Delta B = 1.25$ T. In addition the oscillation amplitude does not increase at high B field, which is expected for a SdH-type oscillation as can be seen in figure 3(a). All of these features suggest that they may originate from a quantum effect in real space. For example, the so-called Ahoronov–Bohm (AB) type oscillations have been observed in *MR* measured on antidot arrays devices fabricated on GaAs quantum wells or graphene sheets, which are also periodic in B [13, 14].

AB-type oscillations in antidot arrays are similar but different from the Ahoronov–Bohm interference observed in a single ring because in the arrays the statistical averaging of a large number of antidots would smear out the conventional AB interference. It was argued that the oscillations in antidot arrays are due to the orbit quantization in a periodic structures, and the periodicity of oscillations is determined by flux quanta per orbit area [13]. In order to further investigate the origin of these *MR* oscillations, we extracted out the oscillatory *MR* of the Bi_2Te_3 antidot arrays from 2 to 20 K (as shown in figure 3(c)). We find that the fast-oscillating signal show very strong temperature dependence, whereas the slow-varying feature persists up to $T = 20$ K. To better visualize the data, we performed fast Fourier transforms (FFT) and obtained the frequency spectrum, as shown in figure 3(d). In the FFT spectrum, the peak centered at the $0.8\,T^{-1}$ (i.e. $\Delta B = 1.25$ T), as indicated by the arrow, quickly smears out when temperature approach 20 K. On the other hand, the FFT peaks near zero periodicity (i.e. the slow-varying background) are much less sensitive to temperature variations. As observed in previous studies on different antidot array systems, these slow-varying features could be due to the pinning of classical cyclotron orbits with the antidot lattice [15]. Since it is a classical effect and depends only on elastic scattering rates, it is less sensitive to the de-coherence process at higher temperatures.

On the other hand, the very strong temperature dependence of the $\Delta B = 1.25$ T oscillations indicates their origin from a non-trivial quantum effect. The periodicity in these oscillations corresponds to one magnetic flux quantum penetrating through a closed conduction loop in the unit cell of a periodic lattice, which is the orbit quantization condition in real space and can be expressed by the following equation: $\Delta B = (h/e)/A$, where A is the loop area. Substituting the periodicity ΔB by 1.25 T, we obtain an effective area of 3.32×10^{-15} m^2, roughly corresponding to a circular circumference of 100 nm. We also notice that in figure 2(c), the phase coherence length of the electrons, i.e. the length an electron can travel before losing its phase information, drops below 100 nm when the temperature is higher than 15 K, exactly where we see the smearing out of these oscillations. Combining all this information points to a very likely origin of these oscillations: electrons coherently interfere over small loops of 100 nm in circumference, and form quantization orbits for all unit cells. Since our antidot circumference is ~500 nm, electrons are unlikely to be circulating them. If we carefully examine the structures of the antidot arrays, we find that the thin bridges connecting two adjacent antidot have the circumference around 100 nm (which is also the part with the highest surface-to-volume ratio). This might be the location

[7] Data between $B = 3$ to 13 T are fitted by a second order polynomial.

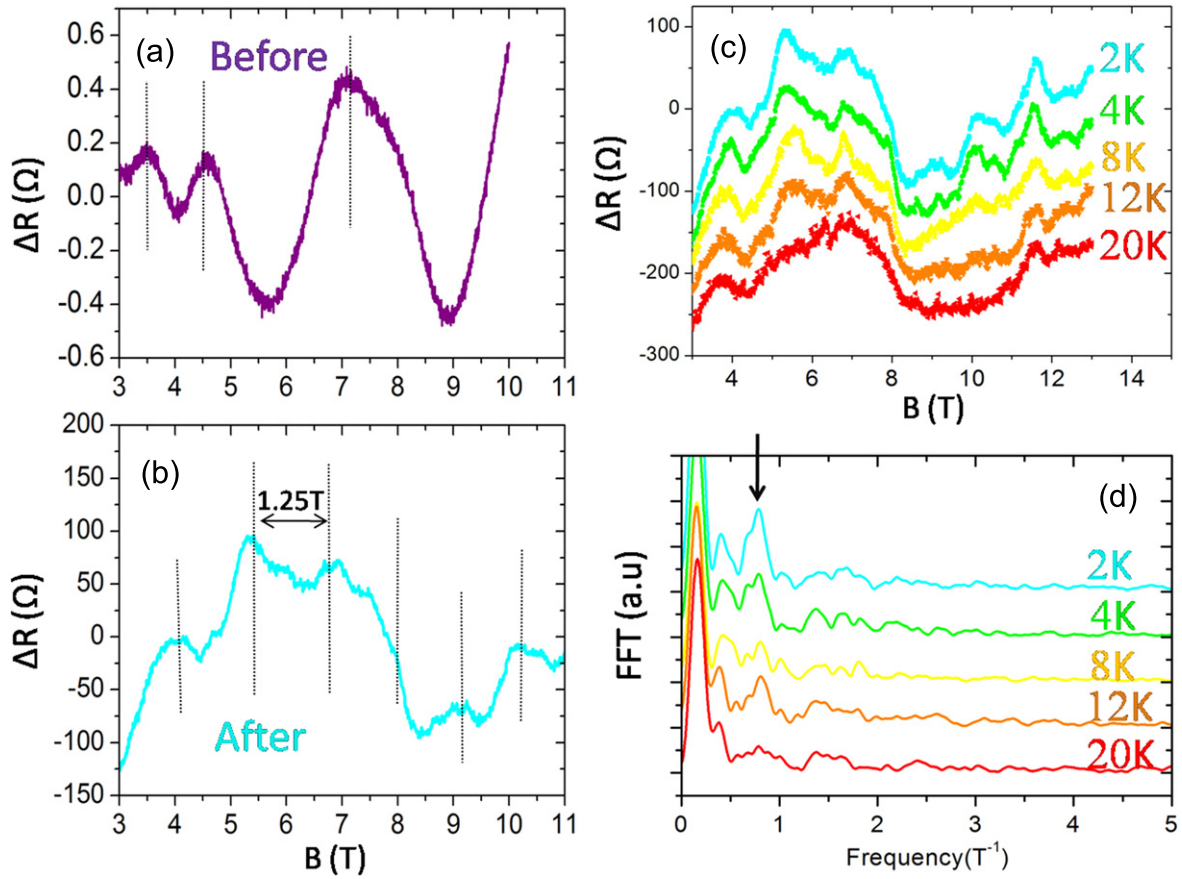

Figure 3. Antidot arrays interacting with charge carriers and modifying the magneto-transport properties of topological insulator Bi_2Te_3. (a) Oscillatory part of the magnetoresistance of the device before and after (b) writing the antidot arrays, obtained by subtracting the smooth polynomial backgrounds for $T = 2$ K. By carefully examining the oscillations, we see that by writing the antidot array, the oscillations of the device changed from Shubnikov–de Haas (SdH) type to Ahoronov–Bohm (AB) type. The oscillation periodicity in microflake scales with B^{-1}, while it stays constant ($\Delta B = 1.25$ T) in antidot arrays. (c) Temperature-dependent study of the magneto-resistance oscillation of the antidot arrays from 2 K to 20 K (background subtracted). (d) Fast Fourier transform spectrum of the data shown in (c). The arrow indicates the prominent oscillation ($\Delta B = 1.25$ T) that shows strong temperature dependence.

the electrons are circulating around and which might be inducing the AB-type oscillations we have observed in the antidot array sample.

4. Conclusions

In summary, we introduced nanosized antidot arrays into a single-crystal Bi_2Te_3 microflake. The antidot arrays increased the surface-to-volume ratio, and manifested the surface conduction effect. Also, the smallest feature size in our antidot arrays is comparable to the coherence length of electrons at low temperatures, as a result, non-trivial AB-type quantum oscillations are observed in our structure. Our study suggests that the electrons in topological insulators can indeed interact with artificially designed nanostructures and significantly modify the transport properties of topological insulators, a more systematic study of the transport behavior of topological insulators as a function of the size and density of anitdot arrays will be highly desirable. Following this direction, we are expecting a wealth of interesting quantum transport phenomena and novel topological insulator–based functional devices to be explored in the future.

Acknowledgments

The authors gratefully acknowledge Professors Junqiao Wu and Sayeef Salahuddin of University of California, Berkeley for their help on this work.

References

[1] Moore J E 2010 *Nature* **464** 194–8
[2] Hasan M Z and Kane C L 2010 *Rev. Mod. Phys.* **82** 3045
[3] Qi X and Zhang S 2011 *Rev. Mod. Phys.* **83** 1057
[4] Zhang Y *et al* 2010 *Nat. Phys.* **6** 584–8
[5] Peng H, Lai K, Kong D, Meister S, Chen Y, Qi X, Zhang S, Shen Z and Cui Y 2010 *Nat. Mater.* **9** 225–9
[6] Childresab I, Tianab J, Miotkowskiab I and Chen Y 2013 *Phil. Mag.* **93** 681
[7] Kašparová J, Drasar C, Krejcova A, Benes L, Lost'ak P, Chen W, Zhou Z and Uher C 2005 *J. Appl. Phys.* **97** 103720

[8] Lee P A and Ramakrishnan T V 1985 *Rev. Mod. Phys.* **57** 287
[9] Analytis J G, Chu J, Chen Y, Corredor F, McDonald R D, Shen Z X and Fisher I R 2010 *Phys. Rev.* B **81** 205407
[10] Baxter D V, Richter R, Trudeau M L, Cochrane R W and Strom-Olsen J O 1989 *J. Phys. (France)* **50** 1673
[11] Chu R, Lu J and Shen S 2012 *Europhys. Lett.* **100** 17013
[12] Kohler H 1976 *Phys. Status Solidi* B **74** 591
[13] Kato M, Endo A, Katsumoto S and Iye Y 2008 *Phys. Rev.* B **77** 155318
[14] Shen T, Wu Y Q, Capano M A, Rokhinson L P, Engel L W and Ye P D 2008 *Appl. Phys. Lett.* **93** 122102
[15] Weiss D, Roukes M L, Menschig A, Grambow P, von Klitzing K and Weimann G 1991 *Phys. Rev. Lett.* **66** 2790